The response of ice-crystal orientation fabric to velocity-gradient perturbations

M. Hay[1], E.D. Waddington[1]

[1]*Department of Earth and Space Sciences, University of Washington*

ABSTRACT. The distribution of crystal orientations of ice grains (the crystal fabric) of a polycrystal has a strong influence on the flow of polycrystalline ice, due to the plastic anisotropy of the individual grains. The fabric is in turn affected by ice flow. Flow on ice-sheet flanks is dominated by shear on horizontal planes, and divide flow is dominated by longitudinal extension. However, other velocity gradient components may also exist due to bed topography, variability in fabric or grain size, or other factors. This can in turn result in a fabric that differs from the fabric that would occur without any such flow disturbances. Indeed, disturbed stratigraphy is commonly observed near the bed of ice sheets. In this paper, we treat these flow disturbances as random but correlated in time, and determine their effects on crystal fabric. These small deviations in velocity gradient from pure shear or simple shear cab induce the development of single-maximum fabrics with off-vertical directions of maximum c-axis concentration. In turn, this has the potential to induce stratigraphic distortion.

INTRODUCTION

An individual ice crystal deforms most easily in shear parallel to the crystal basal plane, orthogonal to the crystallographic c-axis. Deformation on planes in other orientations is on the order of 10 to 100 times harder. Plastic deformation of an ice polycrystal depends on the orientations of its constituent grains (e.g. Azuma 1994), which is described by the c-axis orientation distribution function (ODF). The ODF is a probability distribution of c-axis density often defined on the upper hemisphere (because a c-axis vector $\boldsymbol{c}$ is indistinguishable from $-\boldsymbol{c}$). In this paper, we will instead treat the ODF as an even function

Table 1. List of symbols

Symbol	Definition
q_i	Component of a tensor in index notation
$\boldsymbol{q}$	Same tensor in vector notation
$\boldsymbol{c}$	Ice-crystal c-axis vector
$\psi(\boldsymbol{c})$	Ice-crystal orientation dist. func.
$< q_i >$	Expected value of q_i under ψ
a_{ij}	Component of the structure-tensor $c_i c_j$
A_{ij}	Comp. of the 2^{th} order orient. tensor $< a_{ij} >$
$\mathbb{A}_{ijkl}$	Comp. of the 4^{th} order orient. tensor $< a_{ij} a_{kl} >$
λ_k	A fabric eigenvalue of $\boldsymbol{A}$
$\boldsymbol{\Xi}$	Matrix of eigenvectors of $\boldsymbol{A}$
$\boldsymbol{V}$	Vorticity, or spin, tensor
$\boldsymbol{D}$	Strain-rate tensor
δ_{ij}	Kronecker delta symbol
$\boldsymbol{S}$	Stress tensor
ϵ	A small parameter
$\|\|\boldsymbol{v}\|\|$	Vector magnitude of $\boldsymbol{v}$, $\sqrt{\boldsymbol{v}^T \boldsymbol{v}}$

defined on the entire sphere for mathematical convenience. A polycrystal with an isotropic ODF will have a bulk isotropic response to applied stress. However, polycrystals develop an anisotropic ODF in response to applied strain.

The development of a preferred orientation is guided primarily by intracrystalline slip. There is a tendency for the c-axes to rotate away from the directions of principal extensional strain due to lattice rotation (Azuma and Goto-Azuma, 1996). ODFs are often summarized using orientation (or, moment) tensors (e.g. Svendsem and Hutter 1996), where the n^{th} order moment tensor is the n^{th} order moment of the ODF. Throughout this paper, the indices 1, 2, and 3 will be associated with the x-, y-, and z-directions, respectively. Fabric is usually described using only the second-order orientation tensor $\boldsymbol{A}$. The component of the second-order orientation tensor A_{ij} is the expectation $< c_i c_j >$, where $i, j = 1, 2, 3$. The mean of the ODF (or the first-order orientation tensor in this terminology), $< c_i >$, is always zero because of antipodal symmetry (and likewise for any odd-order tensor). Therefore, A_{ij} is also a component of the covariance tensor of the distribution:

$$\begin{aligned}\mathrm{Cov}(c_i, c_j) &= < (c_i - < c_i >)(c_j - < c_j >) > \\ &= < (c_i - 0)(c_j - 0) > \\ &= A_{ij} \end{aligned} \quad (1)$$

The diagonal elements A_{11}, A_{22}, and A_{33} give a measure of the c-axis concentration on the x, y, and z axes, respectively. Similar to the second-order orientation tensor, the fourth-order tensor is the expected value $\mathbb{A}_{ijkl} = < c_i c_j c_k c_l >$. Since the second-order orientation tensor is symmetric, it is diagonal in the coordinate system defined by its eigenvectors, or fabric principal directions. The diagonal elements are the fabric eigenvalues λ_i. The eigenvalues sum to unity by construction. The three fabric principal directions denote the directions of greatest density (corresponding to the largest eigenvalue), smallest density (the smallest eigenvalue), and a direction orthogonal to the other two. An isotropic fabric has three equal eigenvalues. A girdle fabric (in which there is a band of high concentration along a great circle) has two nearly equal eigenvalues, and one small eigenvalue. A single-maximum fabric has one large eigenvalue, and two small eigenvalues.

If the evolution of the ODF is given by a partial differential equation (PDE) over the sphere, it is possible to derive an ordinary differential equation (ODE) for the evolution of A_{ij}. This is much easier than solving the PDE, whose solution at any given time is a function defined on the sphere, rather than just the six unique elements of the second-order orientation tensor. This substantially reduces computational difficulties. With this approach, Gillet-Chaulet and others (2006) used a Jefferys-type equation for A_{ij}, valid when the c-axes move by basal slip only. Their model works for arbitrary vorticity tensors and velocity gradients. Gödert (2003) developed a similar model incorporating rotary diffusion into the evolution equation for A_{ij}. In this paper, we take a similar approach to Gillet-Chaulet and others (2006).

Fabric development during ice flow is likely a physically deterministic process. However, at any given site, there are uncertainties in strain history, impurity content, initial conditions at deposition, and other factors. We examine how these uncertainties may affect uncertainties in ice flow. Flow inhomogenities can result from numerous sources. On small scales, random variations in fabric strength can in turn induce spatial differences in flow. Near the bottom of the West Antarctic Ice Sheet (WAIS) divide core, some layers have experienced recrystallization, and have a weaker fabric compared to others that have not recrystallized (Fitzpatrick and others, 2014). Durand and others (2007) found an abrupt transition in the ice fabric at EPICA Dome C corresponding to Termination II, suggesting that climate at the time of initial deposition can play a prominent role in in the subsequent development ice fabric. Alley and others (1997) found evidence of "striping" in the GISP2 core, in which elongated areas of grains possessed off-vertical c-axes. In horizontal extension under divide flow, these stripes localize shear within them, and offset layers in the hard surrounding ice. This induces flow disturbances around stripes,

as well as overturning stratigraphic layers. Jansen and others (2016) produced bands similar to observed stripes in strong single-maximum fabrics using the two-dimensional ELLE microstructure model. Regions where the fabric was tilted away from the bulk lattice-preferred orientation toward the direction of shear seeded the formation of the bands. On larger scales, flow disturbances can arise due to basal topography and transient flow, basal-ice accretion (Bell and others, 2014), or various other sources. Thorsteinsson and Waddington (2002) examined the development of low-angle wrinkles in stratigraphic layers in ice sheets. Under simple shear, low-angle wrinkles will steepen, eventually producing overturned folds. Pure shear or vertical uniaxial compression produce the opposite effect, flattening out wrinkles. Near ice divides, simple shear is less prominent compared to pure shear. However, vertical single-maximum fabrics develop under both vertical compression and simple shear. These fabrics make the ice harder under vertical compression, and soft under horizontal simple shear. This may greatly aid the development of stratigraphic disruption in simple shear, because steepening of incipient folds is enhanced, while flattening is reduced.

In this paper, we analyze how small amounts of variability in the velocity gradient can affect crystal fabric. By "variability," we mean small components of the velocity gradient distinct from the dominant background flow (e.g., simple shear in flank flow). The goal is to see whether it is possible to develop large excursions in the ODF in response to small velocity-gradient perturbations. If, as a result of small excursions in the velocity gradient, large, spatially non-homogeneous differences in fabric can develop, they may seed further velocity gradient disturbances and stratigraphic disruption. We do not examine sources of such flow disturbances. Instead, we make the approximation that they are random, but correlated in time. That is, the perturbation at a certain time will be highly correlated to perturbations at sufficiently nearby times.

This paper is split into two main parts. In the first section, we develop a first-order approximation of the effects of a velocity-gradient perturbation on concentrated vertical single-maximum fabrics in flank flow (horizontal simple shear) and divide flow (pure shear). We show that in both cases, small perturbations of the velocity gradient can cause the fabric principal directions to rotate significantly, generating a fabric that would induce a vertical velocity perturbation in both flow situations. In the second section, we expand on the analytical result by numerically solving the Jeffery's-type equation for the evolution of A_{ij} (see next section) perturbed by a small random velocity gradient. We generate confidence intervals of the six unique components of A_{ij} by computing several thousand realizations. The results numerically confirm the analytical observations in the first section.

Fabric evolution

The most important process governing the development of crystal fabrics is deformation-induced grain rotation. If grain deformation is due solely to basal glide, the rate of change of the c-axis orientation is the sum of bulk rotation and viscoplastic spin. From Meyssonnier and Philip (1996), the evolution of c-axis orientation in response to strain can be described by a

modified Jeffery's equation (Jeffery, 1922):

$$\dot{c_i} = V_{ij}c_j - D^g_{ij}c_j + c_i c_j c_k D^g_{jk}, \tag{2}$$

where c_i is the unit vector in the direction of the c-axis. The quantities V_{ij} and D^g_{ij} are components of the rotation-rate tensor, and local strain-rate tensor of the grain, respectively. The first term gives the rotation rate due to the bulk rotation of the polycrystal, while the second term gives the rotation rate due to viscoplastic spin. Thus, for example, the c-axis of a grain experiencing uniaxial compression will rotate towards the compressive direction. The last term of Jeffery's equation (2) ensures that the motion of grain orientation is tangent to the unit sphere at $\boldsymbol{c}$, which is necessary due to the convention that the c-axis vector is of unit length. This can be seen by noting that the $V_{ij}c_j$ term does not affect the magnitude of c_i, leaving only the $D_{ij}c_j$ term. Assume that at time $t = 0$, the c-axis is given by $\boldsymbol{c}_0$. After a short length of time δt, the magnitude of the new c-axis $\boldsymbol{c}_{\delta t}$ is (without the final term in Equation 2),

$$||\boldsymbol{c}_{\delta t}|| = ||\boldsymbol{c}_0 - \delta t \boldsymbol{D}\boldsymbol{c}|| \tag{3}$$

$$\approx ||\boldsymbol{c}_0|| - \boldsymbol{c}_0^T \boldsymbol{D}\boldsymbol{c}_0 \delta t \tag{4}$$

$$= 1 - \boldsymbol{c}_0^T \boldsymbol{D}\boldsymbol{c}_0 \delta t, \tag{5}$$

to first order in δt. Thus, for the c-axis to maintain unit length, we must add the quantity $\boldsymbol{c}^T \boldsymbol{D}\boldsymbol{c}\delta t$ projected onto $\boldsymbol{c}$, by multiplying by $\boldsymbol{c}$. This then gives the last term of Equation (2). Rather than compute the rotation rate for each grain individually, we instead seek an evolution equation for the second-order orientation tensor whose components are given by $A_{ij} =< c_i c_j >$. Differentiating with respect to time, we have,

$$\frac{dA_{ij}}{dt} =< \dot{c}_i c_j > + < c_i \dot{c}_j > . \tag{6}$$

This introduces the problem of homogenization. We must average out the quantity in the brackets over the entire ODF. However, $\dot{c}^k_i$, for some individual grain k, depends on the strain-rate tensor of that particular grain as can be seen in Equation (2). Thus, we need a tractable method for relating the bulk stress and strain to that of individual grains. The stress and strain of each individual grain should ideally be consistent with the bulk stress and strain rate. The two possible end-members are the Taylor-Bishop-Hill model (Taylor, 1938), assuming homogeneous strain among grains, and the Sachs model (Sachs, 1928), which assumes homogeneous stress among grains. Visco-plastic self-consistent (VPSC) homogenization methods (Lebensohn and Tomé, 1993) have been used for anisotropic ice-flow constitutive relations (e.g. Castelnau and others (1997), Gillet-Chaulet and others (2006)). VPSC schemes treat each individual grain as an ellipsoidal inclusion in a medium with the average properties of the polycrystal. This can provide a more accurate distribution of stress and strain within the polycrystal, with stress and

strain both dependent on the orientation of a grain. Grain rotation due to lattice rotation can also be directly incorporated into VPSC schemes. However, VPSC schemes are typically computed iteratively over finite samples of grains, and are difficult to directly incorporate into Eq. (6). As a compromise, Gillet-Chaulet and others (2005) took the strain on an individual grain as a weighted average between the homogeneous stress and homogeneous strain assumption. In this case, D^g_{ij} in Eq. 2 is,

$$D^g_{ij} = (1-\alpha)\bar{D}_{ij} + \alpha\frac{\varsigma\bar{S}_{ij}}{2}, \tag{7}$$

where $\bar{D}_{ij}$ is a component of the *bulk* strain-rate tensor, $\bar{S}_{ij}$ is a component of the bulk stress tensor, and ς is the fluidity for shear parallel to the basal plane. The weighting between homogeneous stress and homogeneous strain is given by the interaction parameter α. Setting $\alpha = 0$ gives the homogeneous strain rate assumption, while $\alpha = 1$ gives homogeneous stress. This parameter may be tuned to fit a VPSC model. In Gillet-Chaulet and others (2006) they used a value of $\alpha = 0.06$. Throughout this paper, we use the homogeneous strain assumption, with $\alpha = 0$. The homogeneous strain assumption for grain rotation produces fairly realistic predictions for fiber orientation, even though the homogeneous strain assumption produces rather poor predictions of ice flow. Given that Gillet-Chaulet and others (2006) found the best results with $\alpha = 0.06$, we are not too far off by setting $\alpha = 0$. Note that setting $\alpha \neq 0$ to yield a local grain strain rate equal to G_{ij} produces the same predictions as assuming homogeneous strain, and setting the bulk strain $\bar{D}_{ij} = G_{ij}$. For vertical single-maximum fabrics forced with simple shear or pure shear, as in this paper, D_{ij} and S_{ij} are proportional with dimensions of viscosity.

With this assumption, the derivative of the second-order orientation tensor $\boldsymbol{A}$ becomes,

$$\frac{dA_{ij}}{dt} = V_{ik}A_{kj} - A_{ik}V_{kj} - D_{ik}A_{kj} - A_{ik}D_{kj} + \mathbb{A}_{ijkl}D_{kl}. \tag{8}$$

The presence of the fourth-order orientation tensor $\mathbb{A}_{ijkl}$ in Eq. (8) introduces the closure problem. In general, $\mathbb{A}_{ijkl}$ cannot be found from $\boldsymbol{A}$. If we used an additional evolution equation for $\mathbb{A}_{ijkl}$, then the six-order orientation tensor would appear in that equation, and so on. Thus, we need some way of approximating $\mathbb{A}_{ijkl}$ in terms of $\boldsymbol{A}$. In this paper, we use the popular and simple quadratic closure, where $\mathbb{A}_{ijkl} = A_{ij}A_{kl}$ (Advani and Tucker, 1990). This closure is exact in the case of perfectly concentrated single-maximum fabrics, where $A_{ij} = \delta_{i3}\delta_{j3}$. It is quite accurate whenever $\lambda_3 > 0.8$ or so. In this paper, we are primarily intersted in the response of strong fabrics to velocity-gradient perturbations, so this is a good approximation for our purposes.

FIRST-ORDER PERTURBATIONS TO STRONG SINGLE-MAXIMUM FABRICS

We now examine the analytic sensitivity of strong vertical-maximum fabrics to velocity-gradient perturbations. We show that fabrics are susceptible to developing "tilted cone" fabrics, in which the direction of greatest concentration is not vertical, in both horizontal pure shear and simple shear. Here we add a small perturbation $\epsilon\hat{A}_{ij}$ to the component of the second-order

Fig. 1. The six unique components of $\boldsymbol{A}$ for 3000 realizations of the Jeffery's-type equation (8) forced with pure shear and a strain perturbation whose components average 2% of the background pure shear, and $\gamma = 1$. The central 95% of realizations are shaded. Significant deviations of A_{13} and A_{23} occur. These correspond to tilted cone fabrics whose direction of greatest concentration differs on the order of 5° from vertical.

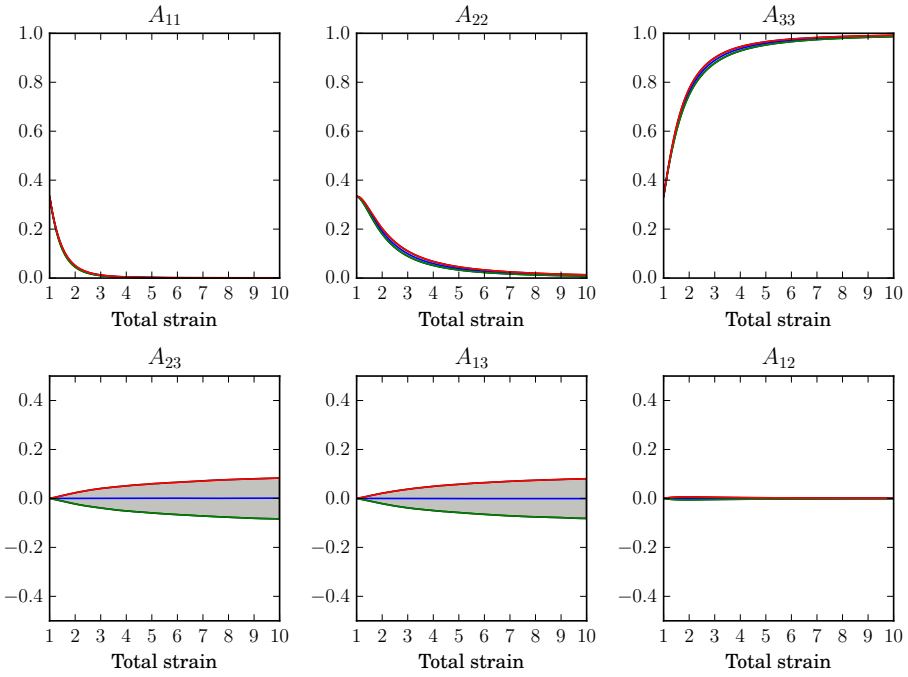

orientation tensor A_{ij}. The tensor $\hat{\boldsymbol{A}}$ has zero trace, and ϵ is small. Then, components of the perturbed second-order orientation tensor are given by $\tilde{A}_{ij} = A_{ij} + \epsilon\hat{A}_{ij}$.

Next, we also assume that the vorticity and strain rate are perturbed by small quantities $\epsilon\hat{\boldsymbol{V}}$ and $\epsilon\hat{\boldsymbol{D}}$, respectively. Then, we can substitute these quantities into Eq. (8), and discard quantities of $\mathcal{O}(\epsilon^2)$ and higher. This then gives us a first-order equation for the perturbed quantities,

$$\frac{d\hat{A}_{ij}}{dt} = \hat{V}_{ik}A_{kj} + V_{ik}\hat{A}_{kj} - \hat{A}_{ik}V_{kj} - A_{ik}\hat{V}_{kj} - \tag{9}$$

$$\hat{D}_{ik}A_{kj} - D_{ik}\hat{A}_{kj} - \hat{A}_{ik}D_{kj} - A_{ik}\hat{D}_{kj} + \tag{10}$$

$$2\left(\hat{A}_{ij}A_{ij}D_{kl} + A_{ij}\hat{A}_{ij}D_{kl} + A_{ij}A_{kl}\hat{D}_{kl}\right) \tag{11}$$

We focus on perturbations to strong single maximum fabrics, common in deeper layers of ice sheets. To express this, we assume that the unperturbed fabric is a perfect vertical maximum ($A_{ij} = \delta_{i3}\delta_{j3}$).

Fig. 2. The six unique components of $\boldsymbol{A}$ for 3000 realizations of the Jeffery's-type equation (8) forced with pure shear and a strain perturbation whose components average 5% of the background pure shear, with $\gamma = 1$. the central 95% of realizations are shaded. Larger deviations of A_{13} and A_{23} occur than under 2% average perturbations. These correspond to tilted cone fabrics tilted on the order of 10° from vertical. The background pure shear is very effective at restraining perturbations of other components of $\mathbf{A}$.

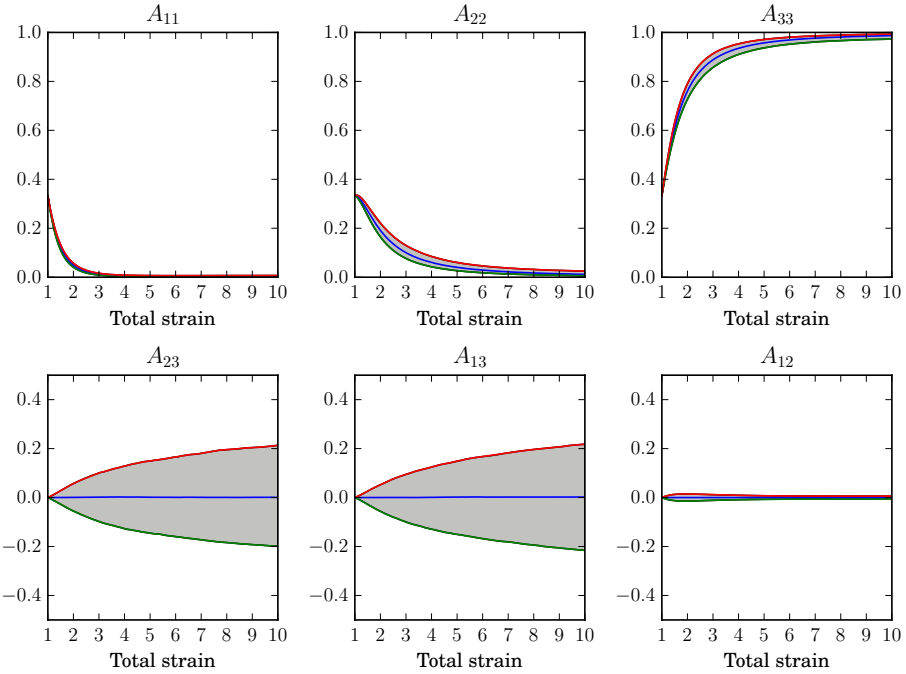

We first look at the case of pure shear. Here, we let $A_{ij} = \delta_{i3}\delta_{j3}$, $D_{ij} = \delta_{i1}\delta_{i1} - \delta_{i3}\delta_{j3}$, and $V_{ij} = 0$. Substituting these quantities into Eq. (9), we get,

$$\frac{d\hat{\boldsymbol{A}}}{dt} = \begin{pmatrix} -4\hat{A}_{11} & -3\hat{A}_{12} & -2\hat{A}_{13} - \hat{D}_{13} + \hat{V}_{13} \\ -3\hat{A}_{12} & -2\hat{A}_{22} & -\hat{A}_{23} - \hat{D}_{23} + \hat{V}_{23} \\ -2\hat{A}_{13} - \hat{D}_{13} + \hat{V}_{13} & -\hat{A}_{23} - \hat{D}_{23} + \hat{W}_{23} & 2(2\hat{A}_{11} + \hat{A}_{22}) \end{pmatrix}, \tag{12}$$

The perturbations $\hat{A}_{11}$, $\hat{A}_{22}$, $\hat{A}_{33}$, $\hat{A}_{12}$, and $\hat{A}_{21}$ are not affected by the perturbed strain and vorticity, to first order. In addition, any initial perturbations in these components decay. Therefore, we do not expect small velocity-gradient perturbations to have a large effect on these components.

The situation is different for A_{13} and A_{23}. The component A_{13} is affected by the components $\hat{D}_{13}$ and $\hat{V}_{13}$ of the perturbed strain and vorticity tensors in the first order. In this case, we expect small velocity-gradient perturbations to induce more significant fabric perturbations.

Now, we will look at simple shear. Again, we let the unperturbed second-order orientation tensor $A_{ij} = \delta_{i3}\delta_{j3}$, corresponding to a perfect single maximum. We also take $D_{ij} = \delta_{i3}\delta_{j1} + \delta_{j3}\delta_{i1}$, and $W_{ij} = \delta_{j3}\delta_{i1} - \delta_{i3}\delta_{j1}$. Substituting these into Eq. (9),

Fig. 3. The six unique components of $\boldsymbol{A}$ for 3000 realizations of the Jeffery's-type equation (8) forced with simple shear and a strain perturbation whose components average 2% of the background pure shear, with $\gamma = 1$. The central 95% of realizations are shaded. Smaller perturbations develop than with pure shear. However, they still may be enough to seed further fabric and flow disturbances.

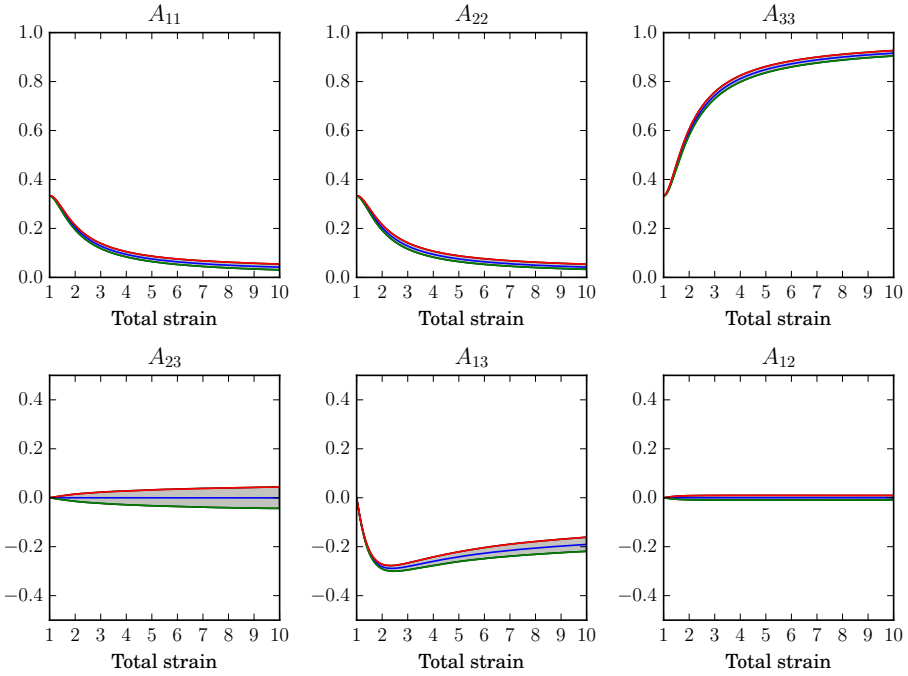

we get,

$$\frac{d\hat{\boldsymbol{A}}}{dt} = \begin{pmatrix} -2\hat{A}_{13} & -\hat{A}_{23} & \hat{A}_{22} - \hat{D}_{13} + \hat{W}_{13} \\ -\hat{A}_{23} & 0 & -\hat{A}_{12} - \hat{D}_{23} + \hat{W}_{23} \\ \hat{A}_{22} - \hat{D}_{13} + \hat{W}_{13} & -\hat{A}_{12} - \hat{D}_{23} + \hat{W}_{23} & 2\hat{A}_{13} \end{pmatrix}. \tag{13}$$

As with the case of pure shear, the only components that are directly affected by velocity-gradient perturbations (to first order) are $\hat{A}_{13}$ and $\hat{A}_{23}$. The growth of the perturbation $\hat{A}_{13}$ to A_{13} is affected by $\hat{A}_{22}$. Depending on the signs of $\hat{D}_{13}$ and $\hat{V}_{13}$, it may be restrained or reinforced by $\hat{A}_{22}$. Similarly, other components depend on each other, to first order. For example, A_{11} depends negatively on A_{13}. However, we may expect that $\hat{A}_{13}$ and $\hat{A}_{23}$ will generally be the largest components of $\hat{\boldsymbol{A}}$ in magnitude. As long as their magnitudes are generally less than the applied velocity-gradient perturbations, perturbations to other components will grow more slowly. For example, if $|-2\hat{A}_{13}|$, the growth rate of the perturbation to A_{11}, is less than $|\hat{A}_{22} - D_{13} + W_{13}|$, the growth rate of $\hat{A}_{13}$, we can expect $\hat{A}_{13}$ to grow faster than $\hat{A}_{11}$. This intuition is confirmed numerically in the next section.

MONTE-CARLO ANALYSIS OF STRESS PERTURBATIONS

We now expand on the sensitivity analysis of the previous section by considering numerical solutions to the Jeffery's equation (8) forced with background simple shear or pure shear in addition to a small random velocity gradient. This gives us an idea of the magnitude of fabric perturbations that we may expect in response to velocity-gradient perturbations. It also allows us to look at the effects of velocity-gradient perturbations away from equilibrium. In the previous section, we showed that background pure shear or simple shear is not effective at restraining perturbations of the A_{13} and A_{23} components of the second-order orientation tensor. Integrating the Jefferys equation (8) through time, we can expect the effects of velocity-gradient perturbations to be magnified, as integration acts as a low-pass filter.

First, we must have some way of generating velocity-gradient perturbations. It is reasonable to assume that a velocity-gradient perturbation at time t will be highly correlated to perturbations at $t+\epsilon$, if ϵ is small enough. To account for this, we construct the velocity-gradient perturbations using realizations of a Gaussian process. A Gaussian process is a random process (or function) $X(t)$ for which any finite sample $(X_{t_1}, X_{t_2}, ..., X_{t_k})$ from the process has a joint Gaussian distribution, determined by a covariance function $C(t_0, t_1)$ which gives the covariance $\mathrm{Cov}(X_{t_0}, X_{t_1}) = C(t_0, t_1)$.

Let $\hat{U}^t_{ij}$ be a component of a realization of the perturbed velocity gradient at time t. To generate $\hat{U}^t_{ij}$, we first sample a realization $G^{t_k}_{ij}$ from the Gaussian process, for each discretized time t_k. Since the time is taken at a discrete number of points, this is just a sample from an ordinary multivariate normal distribution with a mean of zero whose covariance tensor has components given by $K_{ij} = C(t_i, t_j)$.

We assume that G^t_{ij} has a squared-exponential covariance function, $C(t, t') = \sigma^2 \exp(-\gamma(t-t')^2)$. The parameter γ, where $\gamma \geq 0$, controls how closely nearby points are correlated. A small value of γ means that two different points are more highly correlated. Smaller values of γ will tend to promote larger fabric perturbations, since the higher degree of correlation over time will help prevent fabric perturbations from being cancelled out. The quantity σ^2 gives the variance of the perturbation at a single point. The tensor with components G^t_{ij} does not satisfy incompressibility. Incompressibility is recovered by subtracting one third of the trace from each component of the diagonal, yielding the velocity-gradient perturbation $\hat{U}^t_{ij}$.

We plot the central 95% interval of the six independent elements of the tensor $\boldsymbol{A}$ for 3000 realizations of velocity-gradient perturbations under pure shear for perturbations averaging 2% and 5% of background strain, in Figures 1 and 2, respectively. The model is run until reaching a total strain of 10, excluding the velocity-gradient perturbations. Time is nondimensionalized by the strain rate, such that the strain rate is unity. We set $\gamma = 1$, which means that velocity-gradient perturbations occuring at nondimensional times seperated by more than 2 are nearly uncorrelated. The initial fabric is taken to be isotropic, with $A_{11} = A_{22} = A_{33} = 1/3$. Consistent with the analytical results from the previous section, A_{13} and A_{23} have much greater differences between their 2.5% and 97.5% quantiles than other components. This corresponds to the development of a tilted

cone fabric, with A_{13} being the Euler angle of rotation about the x-axis, to first order. Similarly, A_{23} is the Euler angle rotation of the fabric about the y-axis, to first order.

In Figures 3 and 4, we plot the same results for simple shear under 2% and 5% average velocity-gradient perturbations, respectively. Just like the case with pure shear, A_{13} and A_{23} have relatively large spreads between the 2.5% and 97.5% quantiles. Other components are perturbed to a lesser extent, but to a much greater degree than in the case of pure shear. This is most likely because the background simple shear does not restrain the growth of perturbations in any component, to first order (as can be seen in Equation 3).

CONCLUSIONS

Stratigraphic disruption in basal ice is a significant problem for the interpretation of ice-core records. The strong viscous anisotropy of ice may play a significant role in the development of stratigraphic disturbances (e.g. Azuma and Goto-Azuma 1996, Thorsteinsson and Waddington 2002). We showed that ice-crystal orientation fabric is sensitive to velocity-gradient perturbations. In particular, even small velocity-gradient perturbations are capable of producing single-maximum fabrics whose axes of maximum c-axis concentration deviate significantly from vertical. Background pure shear or simple shear is not effective at restraining these perturbations. Such fabrics are capable of inducing layer overturning in response to pure shear (divide flow) or simple shear (flank flow).

There may be numerous sources for stratigraphic disruption in basal ice. The dynamics of basal ice can become very complicated in some settings due to basal freeze-on, recrystallization, and sliding. However, c-axis orientation fabric must always play a role, because any flow which can induce stratigraphic disruption will also affect fabric. We did not consider the coupling of flow and fabric evolution in this paper. Perturbations to fabric cause perturbations to flow, possibly inducing further fabric disturbances. Therefore, this analysis is only appropriate to help understand the onset of disturbances to crystal fabric in response to a velocity-gradient perturbation. More work is needed to understand the coupling of fabric development to ice flow, and other physical processes of basal ice.

ACKNOWLEDGEMENT

This work was supported by the National Science Foundation grants 0944199 and 1246045.

References

Advani, Suresh G and Charles L Tucker, 1990. Closure approximations for three-dimensional structure tensors, *Journal of Rheology*, **34**(3), 367–386.

Fig. 4. The six unique components of $\boldsymbol{A}$ for 3000 realizations of the Jeffery's-type equation (8) forced with simple shear and a strain perturbation whose components average 5% of the background pure shear, using $\gamma = 1$. The central 95% of realizations are shaded. Large deviations in A_{13} and A_{23} occur than with 2% average velocity-gradient perturbations, corresponding to tilted cone fabrics deviating on the order of 5° from vertical. Smaller deviations occur in other components.

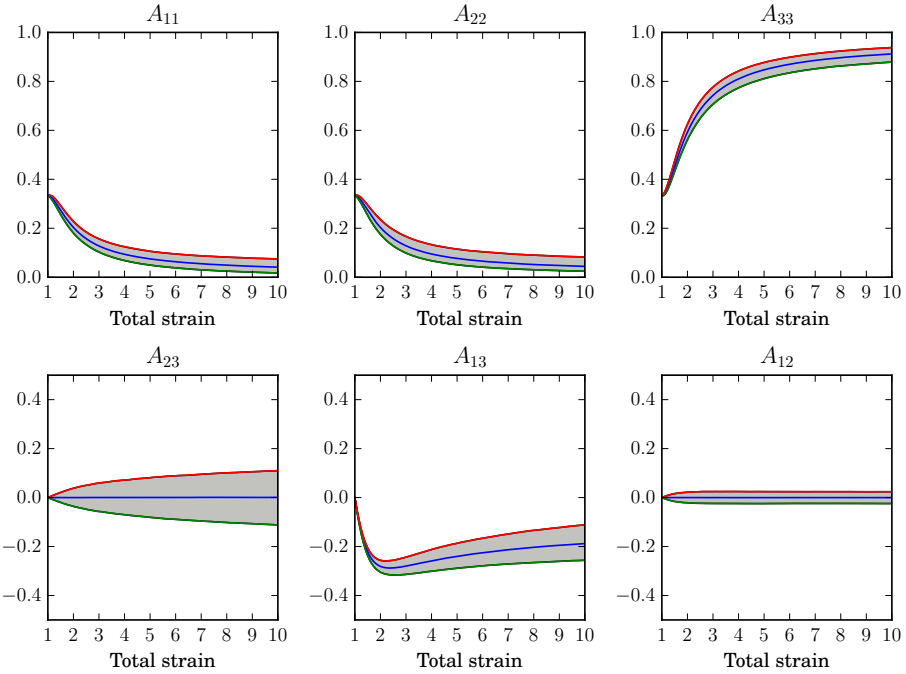

Alley, R.B., A.J. Gow, D.A. Meese, J.J. Fitzpatrick, E.D. Waddington and J.F. Bolzan, 1997. Grain-scale processes, folding, and stratigraphic disturbance in the GISP2 ice core, *Journal of Geophysical Research*, **102**(C12), 26819–26.

Azuma, N., 1994. A flow law for anisotropic ice and its application to ice sheets, *Earth and Planetary Science Letters*, **128**(3-4), 601–614.

Azuma, N. and K. Goto-Azuma, 1996. An anisotropic flow law for ice-sheet ice and its implications, *Annals of Glaciology*, **23**, 202–208.

Bell, R. E., K. Tinto, I. Das, M. Wolovick, W. Chu, T.T. Creyts, N. Frearson, A. Abdi and J.D. Paden, 2014. Deformation, warming and softening of Greenland's ice by refreezing meltwater, *Nature Geoscience*, **7**(7), 497–502.

Castelnau, O., G.R. Canova, R.A. Lebensohn and P. Duval, 1997. Modelling viscoplastic behavior of anisotropic polycrystalline ice with a self-consistent approach, *Acta materialia*, **45**(11), 4823–4834.

Durand, G., F. Gillet-Chaulet, A. Svensson, O. Gagliardini, S. Kipfstuhl, J. Meyssonnier, F. Parrenin, P. Duval, D. Dahl-Jensen and others, 2007. Change in ice rheology during climate variations–implications for ice flow modelling and dating of the EPICA Dome C core, *Climate of the Past*, **3**(1), 155–167.

Fitzpatrick, J., D. Voigt, J. Fegyveresi, N. Stevens, M. Spencer, J. Cole-Dai, R. Alley, G. Jardine, E. Cravens, L. Wilen and others, 2014. Physical properties of the WAIS Divide ice core, *Journal of Glaciology*, **60**(224), 1181.

Gillet-Chaulet, F., O. Gagliardini, J. Meyssonnier, M. Montagnat and O. Castelnau, 2005. A user-friendly anisotropic flow law for ice-sheet modelling, *Journal of glaciology*, **51**(172), 3–14.

Gillet-Chaulet, F., O. Gagliardini, J. Meyssonnier, T. Zwinger and J. Ruokolainen, 2006. Flow-induced anisotropy in polar ice and related ice-sheet flow modelling, *Journal of Non-Newtonian Fluid Mechanics*, **134**(1), 33–43.

Gödert, Günter, 2003. A mesoscopic approach for modelling texture evolution of polar ice including recrystallization phenomena, *Annals of Glaciology*, **37**(1), 23–28.

Jansen, D., M.G.V. Llorens, J. Westhoff, F. Steinbach, S. Kipfstuhl, P.D. Bons, A. Griera and I. Weikusat, 2016. Small-scale disturbances in the stratigraphy of the NEEM ice core: observations and numerical model simulations, *The Cryosphere*, **10**, 359–370.

Jeffery, G.B., 1922. The motion of ellipsoidal particles immersed in a viscous fluid, *Proceedings of the Royal Society of London. Series A, Containing papers of a mathematical and physical character*, 161–179.

Lebensohn, R.A. and C.N. Tomé, 1993. A self-consistent anisotropic approach for the simulation of plastic deformation and texture development of polycrystals: application to zirconium alloys, *Acta Metallurgica et Materialia*, **41**(9), 2611–2624.

Meyssonnier, J. and A. Philip, 1996. A model for the tangent viscous behaviour of anisotropic polar ice, *Annals of Glaciology*, **23**, 253–261.

Sachs, G., 1928. Zur Ableitung einer Fliebedingung, *Z. Vereins Dtsch. Ing.*, **12**(8), 734–736.

Svendsem, B. and K. Hutter, 1996. A continuum approach for modelling induced anisotropy in glaciers and ice sheets, *Annals of Glaciology*, **23**(1), 262–269.

Taylor, G.I., 1938. Analysis of plastic strain in a cubic crystal, *Stephen Timoshenko 60th Anniversary Volume*, 218–224.

Thorsteinsson, T. and E.D. Waddington, 2002. Folding in strongly anisotropic layers near ice-sheet centers, *Annals of Glaciology*, **35**(1), 480–486.